AFRL-AFOSR-VA-TR-2016-0146

Influence of Mechanical Loading on the Integrity and Performance of Energy Harvesting and Storage Materials at the Micron and Submicron Scales

Ioannis Chasiotis
UNIVERSITY OF ILLINOIS CHAMPAIGN

04/01/2016
Final Report

Air Force Research Laboratory
AF Office Of Scientific Research (AFOSR)/ RTB2
Arlington, Virginia 22203
Air Force Materiel Command

UNIVERSITY OF ILLINOIS
AEROSPACE ENGINEERING

Final Performance Report

Reporting Period: 6/15/2012 - 12/14/2015

Influence of Mechanical Loading on the Integrity and Performance of Storage Materials at the Micron and Submicron Scales

PI: Ioannis Chasiotis

Aerospace Engineering
University of Illinois at Urbana-Champaign

Talbot Lab, 104 S. Wright Street, Urbana, IL 61801

Telephone: (217) 244-1474, Fax: (217) 244-0720, E-mail: chasioti@illinois.edu

AFOSR Grant # FA9550-12-1-0209

Program Manager: Dr. B.L. Lee

April 1, 2016

REPORT DOCUMENTATION PAGE

Form Approved
OMB No. 0704-0188

1. REPORT DATE *(DD-MM-YYYY)*	**2. REPORT TYPE**	**3. DATES COVERED** *(From - To)*
04/01/2016	FINAL PERFORMANCE REPORT	6/15/2012 - 12/14/2015

4. TITLE AND SUBTITLE

Influence of Mechanical Loading on the Integrity and Performance of Energy Harvesting and Storage Materials at the Micron and Submicron Scales

5a. CONTRACT NUMBER

5b. GRANT NUMBER
FA9550-12-1-0209

5c. PROGRAM ELEMENT NUMBER

6. AUTHOR(S)

IOANNIS CHASIOTIS

Aerospace Engineering, U. Illinois at Urbana-Champaign, M/C 236
306 Talbot Lab, 104 South Wright St., Urbana, IL 61801

5d. PROJECT NUMBER

5e. TASK NUMBER

5f. WORK UNIT NUMBER

7. PERFORMING ORGANIZATION NAME(S) AND ADDRESS(ES)

UNIVERSITY OF ILLINOIS
Aerospace Engineering
104 South Wright St.
Urbana, IL 61801

8. PERFORMING ORGANIZATION REPORT NUMBER

9. SPONSORING / MONITORING AGENCY NAME(S) AND ADDRESS(ES)

Air Force Office of
Scientific Research (AFOSR)
Program: Mechanics of
Multifunctional Materials and
Microsystems

10. SPONSOR/MONITOR'S ACRONYM(S)
Program Manager:
Dr. B.L. Lee

11. SPONSOR/MONITOR'S REPORT NUMBER(S)

12. DISTRIBUTION / AVAILABILITY STATEMENT

Approved for public release

13. SUPPLEMENTARY NOTES

14. ABSTRACT

The mechanical reliability and efficiency of thin film photovoltaics attached to structural members depends on the initial residual stresses in the films. In this research, accurate predictions of the mechanical and functional failure of photovoltaic films co-cured on carbon fiber composite laminates were made possible by quantifying the mean and gradient residual stresses and the failure properties of individual layers in thin film amorphous Si photovoltaics. The experimental results were employed to predict the onset of fragmentation in the transparent conductive oxide ZnO layer and the amorphous Si and the initiation of functional degradation of photovoltaic films co-cured on 0° carbon fiber composite laminates. In parallel, this research program investigated the electrochemical and mechanical performance of graphite and Sn composite anodes subjected to electrochemical cycling. Most composite anodes reported in literature are very porous because they are manufactured from slurry, and as a result, they have no mechanical integrity. The composite graphite and Sn anodes fabricated in this research were prepared by hot pressing which allowed for control of their porosity between 35% and 75%. Porosities larger than 45% preserved the electrochemical capacity of the anodes, as opposed to those with porosities smaller than 40% that had reduced electrochemical capacity. Graphite anodes with ~45% porosity demonstrated the highest retention of tensile strength and elastic modulus after 30 electrochemical cycles, representing an optimum condition. Finally, the fracture of Si as high capacity Li^{+} host material was investigated using Si microsprings. Experiments conducted under purely chemical lithiation, showed good lithiation and small propensity for crack formation, thus making films of such springs a viable material for high capacity thin film anodes.

15. SUBJECT TERMS

16. SECURITY CLASSIFICATION OF:			**17. LIMITATION OF ABSTRACT**	**18. NUMBER OF PAGES**	**19a. NAME OF RESPONSIBLE PERSON**
					Ioannis Chasiotis
a. REPORT	**b. ABSTRACT**	**c. THIS PAGE**			**19b. TELEPHONE NUMBER** ***(include area code) (217) –244-1474***
unclassified	unclassified	unclassified		21	

Standard Form 298 (Rev. 8-98)
Prescribed by ANSI Std. Z39.18

FINAL TECHNICAL REPORT

This report provides an overview of the research undertaken during this research project and the results and conclusions. This research program focused on the mechanics of materials employed in thin film solar cells for energy harvesting, and composite anodes with high capacity Li^+ host materials. For brevity, this report summarizes and discusses the experimental results and references are provided to publications for further details.

1. MECHANICAL DURABILITY OF THIN FILM SI SOLAR CELLS

We investigated the failure process of photovoltaic (PV) amorphous Si thin film solar cells using commercial solar cell modules PT15-300 manufactured by Iowa Thin Film Technologies Inc. (Ames, IA). The dimensions of as-received PV modules were 270×325 mm^2 with total power of 3.08 W and current and voltage of 200 μA and 15.4 V, respectively. The PV films were encapsulated in 1-mm thick Tefzel/EVA, and comprised (Figure 1, top to bottom) of a 1 μm thick ZnO TCO layer, an 1 μm thick amorphous Si p-n junction diode, a 0.1 μm thick conductive polyimide Kapton™ layer acting as the bottom electrode, and a 50 μm thick aluminum substrate. A metallic grid on the surface of the TCO acted as the top electrode.

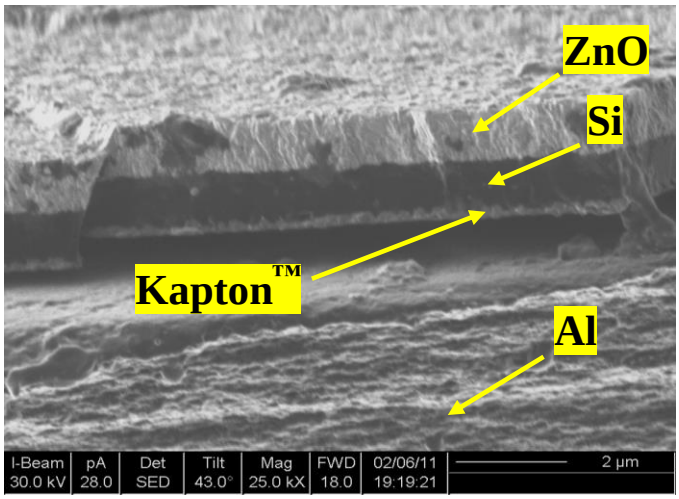

Figure 1. Cross-section of layers in an amorphous Si photovoltaic cell.

1.1. Measurement of Mean and Gradient Stresses in Si and Si/ZnO Films

The mechanics of blister and telephone cord delamination were employed to extract the mean stress in the layers comprising the PV film in Figure 1. Figure 2(a) shows a straight blister and Figure 2(b) a telephone cord blister induced to the films as described in [1]. The mean residual stress driving the formation of straight delamination blisters was calculated by approximating the delaminated segments as clamped-clamped beams [2]. Knowledge of the blister profile geometry allowed for the calculation of the buckling and the residual stresses [2-4]. Specifically, Hutchinson and Suo [2] approximated the delaminated segment of a straight blister as a clamped-clamped buckled beam, while the work in [5] approximated the delaminated segment of a telephone cord blister as a segment of a pinned circular buckle. It has been shown that telephone cord delaminations form instead of straight delaminations when the residual-to-buckling stress ratio is at least four [5], which is the case shown in Figure 2(b).

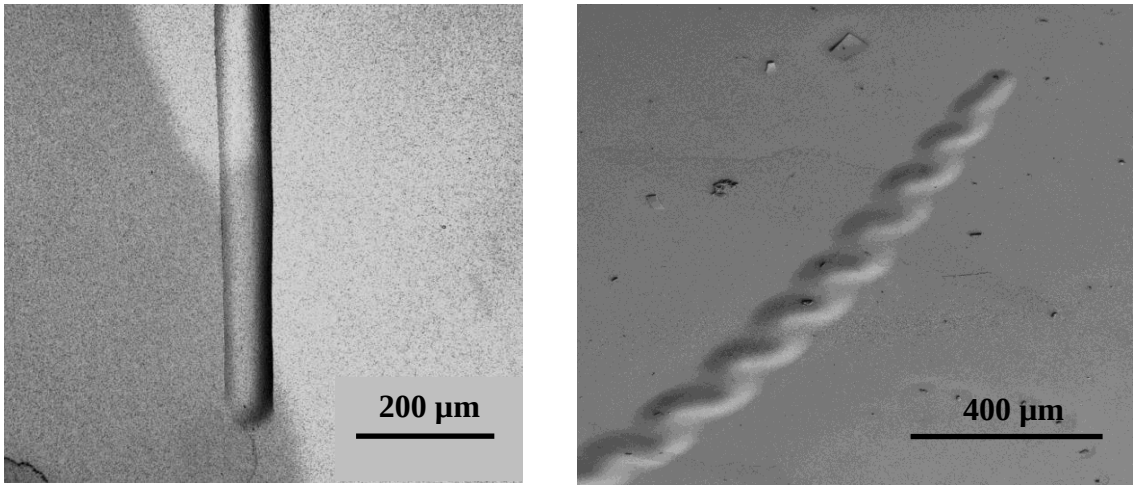

Figure 2. (a) Straight delamination blister, and **(b)** telephone cord delamination blister.

In this study, the blister height and width were measured with a confocal laser scanning microscope and the buckling and mean residual stresses were calculated by the expressions derived in [2,5], which require knowledge of the average elastic moduli of the Si and the ZnO films, their Poisson's ratios, the blister height, and the blister half-width. The elastic moduli and

the true tensile strength of amorphous Si and ZnO films were obtained from microscale tension experiments described in a later Section. In the absence of the ZnO layer, only straight blisters formed in the Si layer, Figure 2(a), as opposed to telephone cord delamination blisters that formed in the Si/ZnO bilayer, Figure 2(b). The formation of telephone cord delamination blisters implied that the deposition of ZnO layer increased the mean compressive stress. Freestanding strips of the Si monolayer and the Si/ZnO bilayer were used to extract the residual stress gradient in the films. The strips exhibited uniform curvature throughout their length which provided support for the presence of a linear stress gradient. The curvature of the Si/ZnO and Si strips indicated that, in the as-deposited state, the top film surface was under tension and the bottom under compression. The radius of curvature and the width of the freestanding strips were measured from images obtained with a confocal laser scanning microscope and a linear stress gradient was calculated by using the Euler-Bernoulli theory.

1.2. Residual Stresses in Si and Si/ZnO Thin Films

Using the profiles of straight and telephone cord delaminations and the models in [2,5], the buckling and mean residual stresses in the Si monolayer and the Si/ZnO bilayer were calculated from a large number of experiments. The buckling stress of the Si monolayer measured from straight delamination blisters was (-159±52) MPa and the mean residual film stress was (-466±118) MPa. Similarly, the buckling stress of the Si/ZnO bilayer measured from telephone cord delamination blisters was (-114±27) MPa and the mean residual stress was (-661±93) MPa. These values correspond to a composite stress since Si and ZnO have different elastic moduli. The stress gradients in the monolayer and the bilayer freestanding strips were calculated by treating the strips as beams subjected to a bending moment. The linear stress gradient calculated from several Si strips was 274±20 MPa/μm. The Si/ZnO bilayer strips were modeled as composite beams, since they consisted of two materials with different elastic moduli, which resulted in a discontinuity in the linear stress gradient in the bilayer. The tensile stress at the top ZnO surface was 360±27 MPa, while the compressive stress at the bottom Si layer was (-319±24) MPa. Figure 3 shows the mean and the gradient stress in the Si/ZnO bilayer as attached to the substrate. The dashed line in Figure 3 corresponds to the neutral axis of the composite beam, which was only 0.06 μm away from the interface inside the ZnO layer. Only the ZnO

layer experienced tensile stresses due the stress gradient, while the entire Si layer was under compression. Yet, the significant tension at the top ZnO surface, owed to the linear stress gradient, was overcome by the large mean compressive stress, thus maintaining the entire Si/ZnO bilayer under compression.

The elastic moduli of the Si and ZnO thin films used in the mean and gradient stress calculations were obtained from microscale tension experiments [6]: The elastic modulus of amorphous Si films was 94±6 GPa which is in good agreement with the value of 94±10 GPa reported in [7]. The tensile strength was 425±75 MPa corresponding to 0.45±0.07% strain at film fracture. The composite modulus of the Si/ZnO specimens was 107±7 GPa and the tensile strength was only 109±23 MPa, which is significantly lower than that of the Si strips, resulting in a maximum allowable strain in the bilayer of only 0.1±0.02%. The elastic modulus of the ZnO films was determined from the Si/ZnO composite modulus and the elastic modulus of the Si monolayer, as 120±7 GPa. This value is within the range of 111 - 137 GPa that has been previously reported, mainly from indentation experiments [8-11].

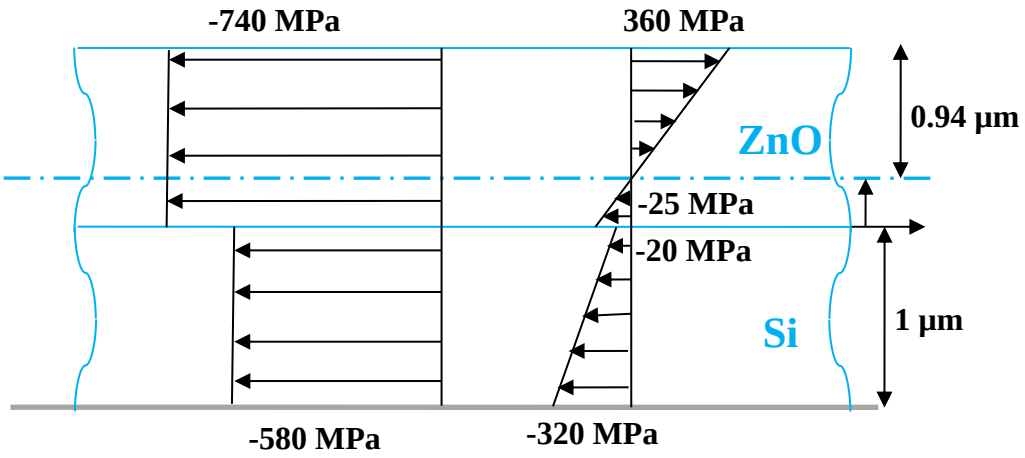

Figure 3. Mean residual stress and stress gradient in a Si/ZnO bilayer attached to Al substrate. The stress values are rounded and the distributions are not drawn to scale.

The stress state in the Si and Si/ZnO films at failure while they are firmly attached to a substrate, e.g. a composite laminate, can be calculated by using the measurements for the mean and gradient residual stresses, and the tensile strength. The significant compressive mean stress in the bilayer, as shown in Figure 3, requires an equal amount of tension to be applied via the substrate. In the case of the Si monolayer, the substrate stress must overcome the initial compressive stress in the Si monolayer (-470 MPa), and the tensile strength of the Si layer (425 MPa) which totals 895 MPa and corresponds to 895/96,000 ≈ 0.9% substrate strain. In order to induce fracture to the ZnO layer, the substrate stress must overcome the initial compressive stress in the ZnO layer (740 MPa) and its tensile strength (110 MPa) which corresponds to an applied strain of 850/120,000 ≈ 0.7% via the substrate. The Si/ZnO strips tested in tension were obtained by relatively complete fragmentation of the PV film via bending. Naturally, wider ZnO fragments appear at smaller strains and, therefore, the estimate of 0.7% substrate strain is good for nearly complete fragmentation of the ZnO film.

1.3. Performance of PVs Integrated on Composite Laminates

The predictions for PV film failure based on the experimental results at the thin PV film level were compared to film fragmentation and photovoltaic efficiency measurements on PV films co-cured with a carbon fiber pre-preg (DA 409U/G35 150 unidirectional carbon fiber). The details of the curing process are described in [1]. The performance and functional degradation of PV films for different values of strain was quantified by using the fill factor (FF). For reference, the FF of a properly functioning PV must be larger than 0.6. PVs with lower FF demonstrated rapid functional degradation during tension testing, potentially due to pre-existing defects. In 0º laminates, fragmentation of the ZnO layer in the form of parallel cracks began at strains as low as ~0.4% with very early signs of fracture appearing at 0.3% strain, as pointed out in Figure 4(a). This value of strain that resulted in the very first cracks in the ZnO layer agreed very well with calculations based on the aforementioned measurements of film stresses and strength. Fragmentation of the ZnO layer was completed at ~0.8% strain, Figure 4(b). Notably, there was no functional degradation of the PVs until complete fragmentation of the ZnO layer. For PV films co-cured with ±45º composite laminates, fragmentation commenced at ~0.25% strain, as

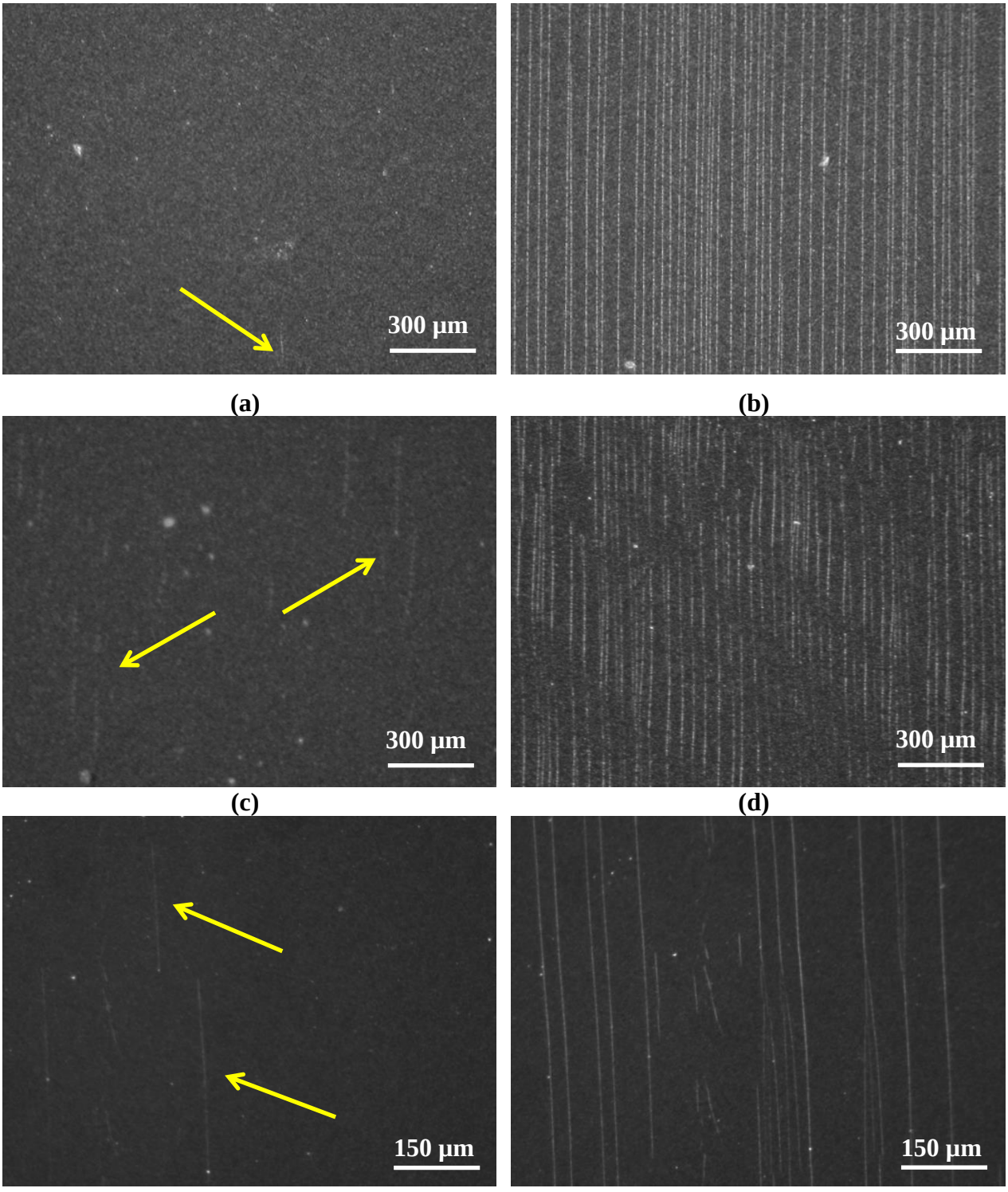

Figure 4. Fragmentation of ZnO layer of a PV film integrated on a 0º laminate subjected to **(a)** 0.3% and **(b)** 0.8% strain. Fragmentation of ZnO in a PV film integrated on a ±45º composite laminate that was subjected to **(c)** 0.25% and **(d)** 0.85% strain. Fragmentation of Si layer in a PV film integrated on a 0º composite laminate subjected to **(e)** 0.7% and **(f)** 0.85% strain.

shown in Figure 4(c), and was completed at ~0.85% strain, Figure 4(d). Fiber shearing in ±45º composite laminates resulted in warping of the PV films, Figure 4(d), which could be responsible for the slightly smaller strain at which cracks formed in the PVs attached to ±45º composite laminates compared to 0º laminates. Experiments with PV films with only the Si layer, which were co-cured with 0º composite laminates, provided further evidence that only the ZnO layer participated in the fragmentation process shown in Figures 4(a-d). The previously computed substrate strain of ~0.9% that was required to cause Si fracture (after ZnO failure) agreed well with the results in Figure 4(e) and Figure 4(f) showing the surface of the Si layer of a PV co-cured with a 0º composite laminate subjected to 0.7% and 0.85% strain, respectively. As mentioned, the microscale tension experiments employed specimens which were already the result of complete fragmentation and their failure strain should be compared to the strain at which the fragment size becomes comparable to the specimen width in microscale tension tests. Notably the prediction of 0.7% substrate strain at failure of the ZnO layer agrees well with the composite strain, Figure 4(b), at which the average width of the fragments was comparable to the average width of the Si/ZnO strips used in microscale experiments, namely ~30 μm. Figure 5 shows the average fragment width vs. (%) strain, showing that the terminal strain for the formation of 30-μm wide fragments is ~0.82%. The same specimen width was used in microscale tension experiments which, as mentioned above, predicted a critical strain value of 0.7%. The difference of 0.12% is actually due to the additional compressive stress generated in the PV films during the curing cycle because of matrix shrinkage: To measure this additional compressive stress, telephone cord delamination blisters were induced to the PV surface after curing. The results showed practically no increase in the buckling stress, while the mean residual stress of the composite Si/ZnO film increased by ~20% to 130 MPa, which corresponds to an additional mean compressive strain of 130/107000 = ~0.12%.

The FF vs. applied strain for a 0º laminate is plotted in Figure 6(a), and for a ±45° laminate in Figure 6(b). The plots show a gradual reduction in the FF for strains larger than 0.8%, which is approximately when fragmentation of the ZnO layer ended and fragmentation of the Si layer began. This gradual reduction in the FF value continued until strain values as high as 1.6%, when the composite laminate failed. At those strains the FF dropped to ~0.3 and 0.1, for 0º and ±45º composite laminates, respectively. It should be noted that the composite strain levels

resulting in fragmentation of the ZnO and Si layers and power output decrease did not change for PV films oriented at different angles with respect to the loading direction.

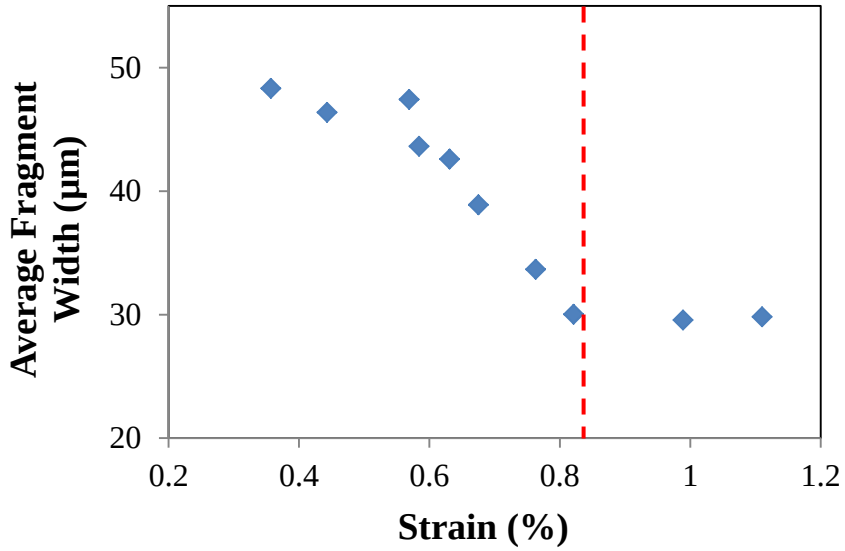

Figure 5. Average fragment width vs. applied substrate strain for a PV attached to a 0º composite laminate.

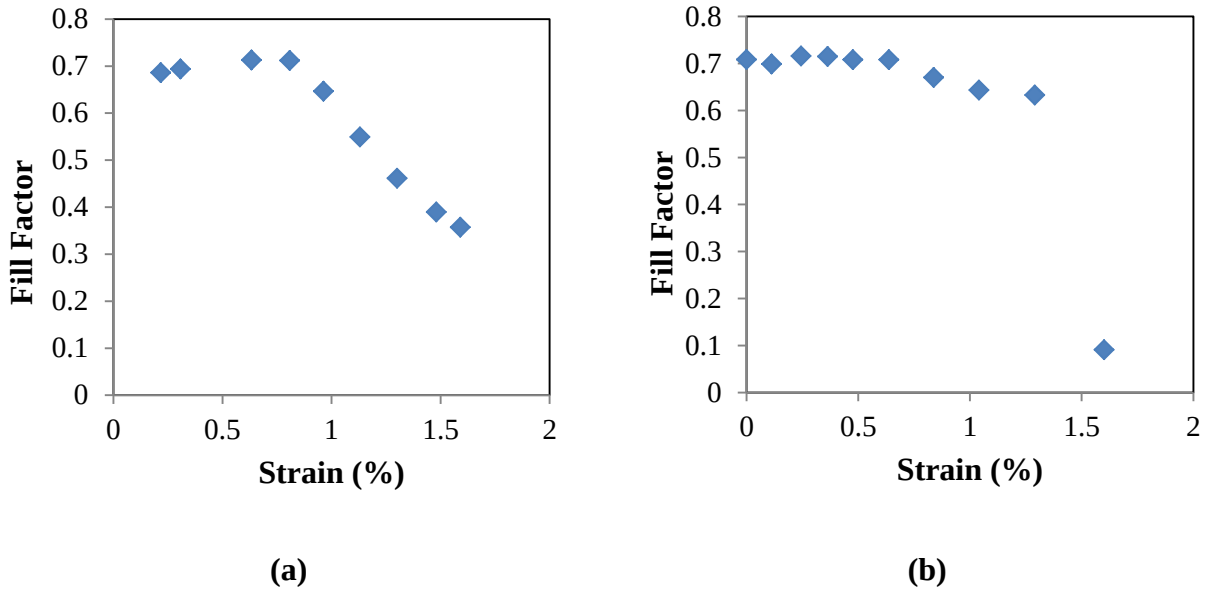

Figure 6. Fill factor vs. applied composite laminate (substrate) strain for a PV co-cured on a **(a)** 0º, and **(b)** ±45º laminate.

1.4. Summary

In summary, the initial stress state of amorphous Si thin film PVs was shown to play an important role in determining their mechanical and functional failure after integration with load bearing structures. The residual stress gradient in the Si and the Si/ZnO layers is very significant, generating quite large tensile stresses at the film's top surface. However, this tensile stress is counteracted by large compressive mean stresses which provide the mechanical integrity of Si/ZnO bilayers, which otherwise can withstand only 0.1% tensile strain in their freestanding configuration. Thus, the mean compressive residual stress is of paramount importance in the load-bearing capacity of amorphous Si PV films. It was also shown that the ZnO layer is the weak link in the Si/ZnO bilayer, with small adhesion to the Si layer. Knowledge of the PV film stress state in its as-deposited form and its tensile properties in freestanding form allowed for predictions of the failure strain of the ZnO and the Si layers when the PV films were co-cured with carbon fiber composite laminates. Fragmentation of the ZnO layer began at laminate strains as low as 0.3% for the 0° laminate and 0.25% for the ±45° laminate, and was almost complete by the time cracks appeared in the Si layer for substrate strains of 0.8%. Fracture of the ZnO layer alone had negligible effect on the PV efficiency. The first signs of functional degradation occurred at substrate strains larger than 0.8%, which agrees with the critical strain for fracture initiation in the Si layer.

2. MECHANICAL INTEGRITY OF COMPOSITE Si ANODES

Composite anodes were prepared by hot-pressing at 360 ºF, which allowed for precise control of their density. The binder was a mix of PVDF and acetylene black (AB) in a ratio of 7:3 wt. and the active material (graphite or Sn) was added in a 1:1 wt. ratio, resulting in composites consisting of 50% wt. active material, 35% wt. binder and 15% wt. conductive material. These weight ratios produced anodes with initial mechanical robustness and good electrical conductivity. Further details about the composition of the anodes and the manufacturing process are provided in [12].

2.1. Mechanical and Electrochemical Property Measurements of Composite Anodes

The mechanical and electrochemical performance was investigated as a function of effective open porosity of the anode, which is accessible by the electrolyte for Li^+ transport. The electrochemical performance of the composite anodes was assessed by measurements of the electrode capacity in the first 2 lithiation/delithiation cycles, which was normalized by the estimated mass of graphite or Sn. Microscale Sn particles have been shown to suffer from degradation after the first few cycles and, therefore, the capacity fade of graphite anodes was evaluated by subjecting them to 2 galvanostatic lithiation/delithiation cycles at rates of C/10 and C/30, followed by 28 cycles at C/5. It should be noted that the capacity measured in the first cycle is not a good measure because is affected by the formation of SEI, which also influences subsequent electrochemical cyclability [13]

Electrochemical cycling was limited to the voltage range of 0.01 - 1.5 V. Two anode shapes were tested: (a) circular with diameter of 5/16 in., and (b) 1 mm wide rectangular strips which were used for mechanical testing. The anodes were placed in a Swagelok-type cell, with Li metal foil acting as the counter-electrode and a Celgard film acting as the separator. The anodes were dipped in electrolyte consisting of 1 M lithium perchlorate ($LiClO_4$) in a 1:1 ethylene carbonate (EC) and DMC solution. Electrochemical testing was not initiated until 1 hr after assembling the Swagelok to allow for the electrolyte to thoroughly wet the composite anode. The entire process of assembling the Swagelok cells was conducted in an Ar filled glove box to prevent oxidation of the Li metal foil and the electrolyte. Once electrochemical cycling was completed, the residual electrolyte was removed by rinsing the anodes in a 1:1 propylene carbonate (PC) and DMC solution.

The binder material undergoes expansion upon wetted by the electrolyte and intercalation of Li^+ into graphite or Sn [14]. This volumetric expansion must be accommodated without particle or matrix fracture which would negatively impact the electrochemical performance of a battery. The elastic modulus, tensile strength and ultimate tensile strain of composite anodes with various porosities were measured in tension with a method as described in [6,15]. Specimens from three types of anodes were tested: (a) PVDF with AB (7:3 wt.) serving as the control material, (b) composite anodes with graphite/PVDF/AB (50:35:15 wt.), and (c) composite anodes with Sn/PVDF/AB (50:35:15 wt.).

2.2. Mechanical Integrity of Composite Anodes after Electrochemical Cycling

The mechanical behavior of composite anodes was evaluated after electrochemical cycling. Specimens of graphite and Sn anodes of various porosities were subjected to electrochemical cycling and subsequently tested in tension. Figures 7(a-d) show the stress vs. strain curves of unlithiated and electrochemically tested anodes after 30 cycles. For porosities between 40% and 50%, the graphite anodes exhibited up to 85% retention of the initial mechanical strength before electrochemical cycling, which was accompanied by increase in ultimate strain. On the contrary, specimens with higher or lower porosity (above 65% and below 40%, respectively) consistently demonstrated poor mechanical property retention after electrochemical cycling. Specimens with low initial porosity largely retained their initial elastic moduli. However, their tensile strength and ultimate strain decreased due to sporadic crack formation owed to PVDF swelling during lithiation [16,17]. Renganathan et al. [18] modeled the stresses generated upon intercalation of graphite particles and showed that a reduction in porosity from 60% to 30% results in 100% increase in the tractions on the graphite particles, which increase the propensity for particle debonding and crack formation in the binder upon cycling.

Graphite anodes with 47% porosity were tested in tension after ½, 1, 2, 5 and 10 electrochemical cycles under galvanostatic conditions. The first two cycles were conducted at C/30 while the rest were conducted at C/5. The reduction in tensile strength and the elastic modulus after the first full cycle is evident in Figures 8(a,b). The tensile strength remained constant in the first full cycle, with an average value of 5.4±0.8 MPa, corresponding to 8% reduction compared to unlithiated samples. Additional electrochemical cycles further reduced the tensile strength to 2.4±0.5 MPa, which corresponds to 58% reduction compared to unlithiated specimens. The reduction in tensile strength was due to matrix crack formation and debonding of the active material from the binder due to local volumetric expansion/reduction of the active material during lithiation/delithiation, as well as the infiltration of the electrolyte in the anode causing the binder to swell [16-19]. The average elastic modulus after the first full cycle was 4.2±0.4 GPa, which was 10% smaller than the as-fabricated anodes. After the second full cycle and for all subsequent cycles the elastic modulus assumed a constant value of 2.0±0.3 GPa, namely a 58% drop compared to as-fabricated anodes. This increase in composite compliance and reduction in tensile strength are consistent with the formation of microcracks and graphite

particle debonding after the completion of the first full lithiation/delithiation, which did not change with additional electrochemical cycling.

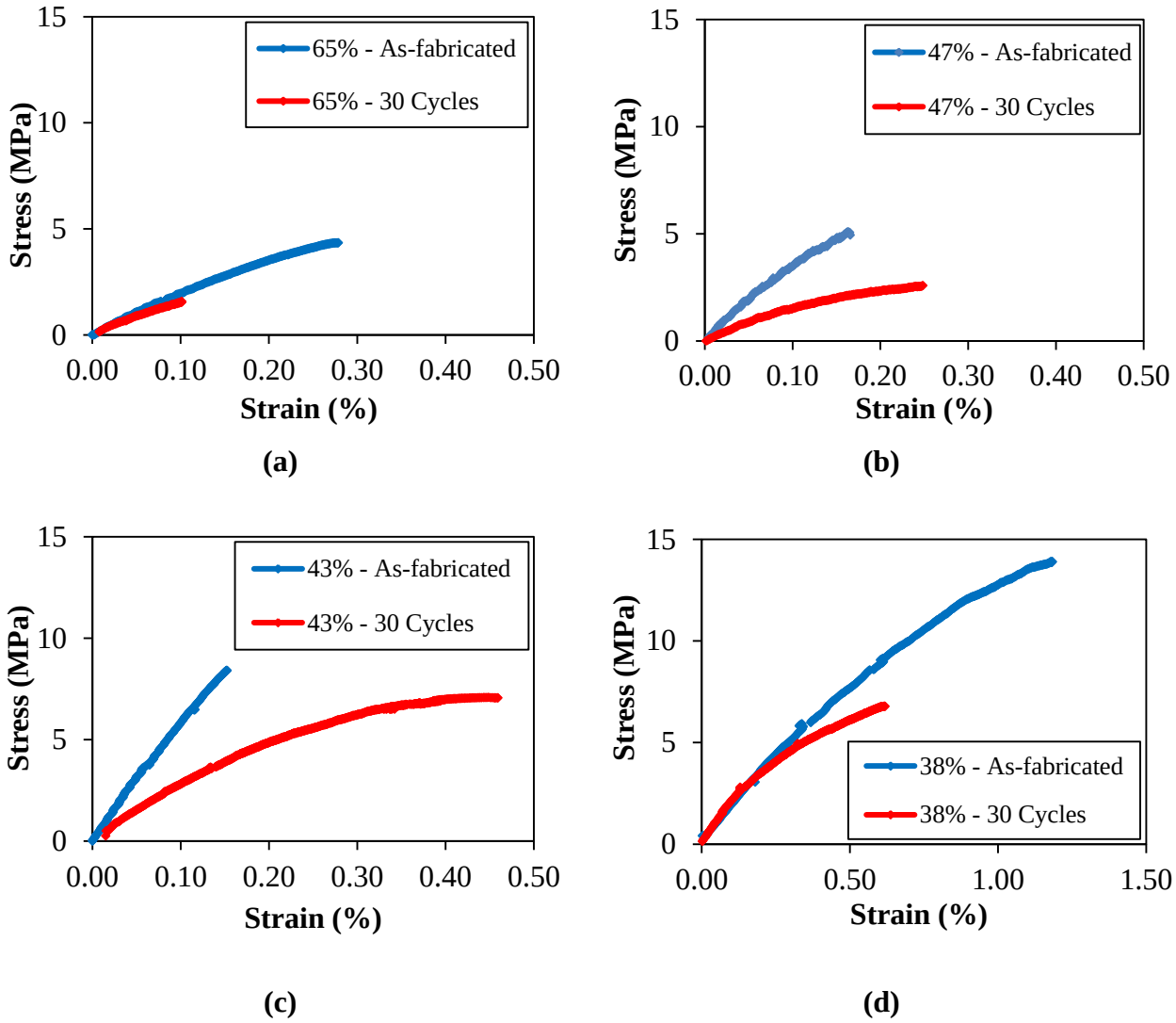

Figure 7. Stress vs. strain curves of as-fabricated and electrochemically cycled graphite anodes with **(a)** 65%, **(b)** 47%, **(c)** 43% and (**d)** 38% porosity.

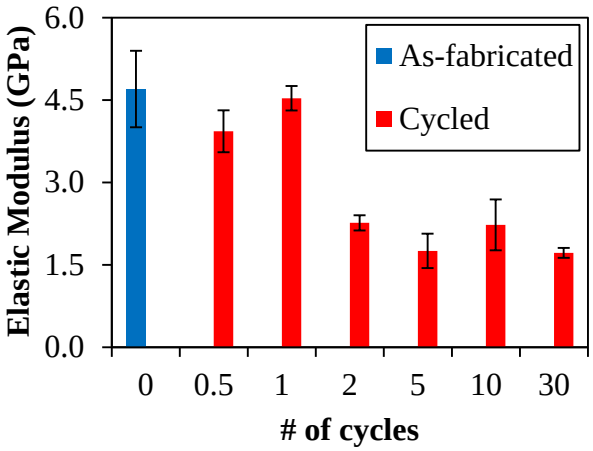

(a)

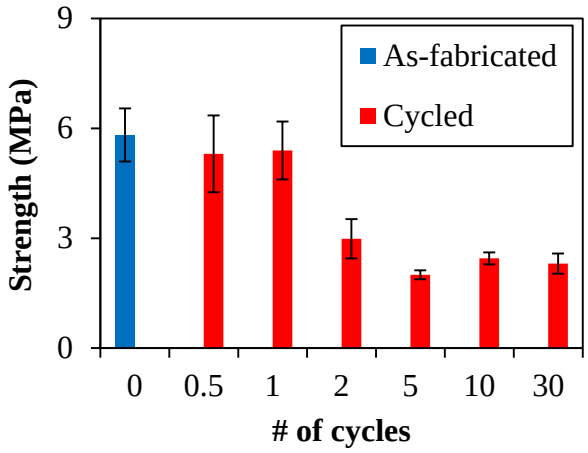

(b)

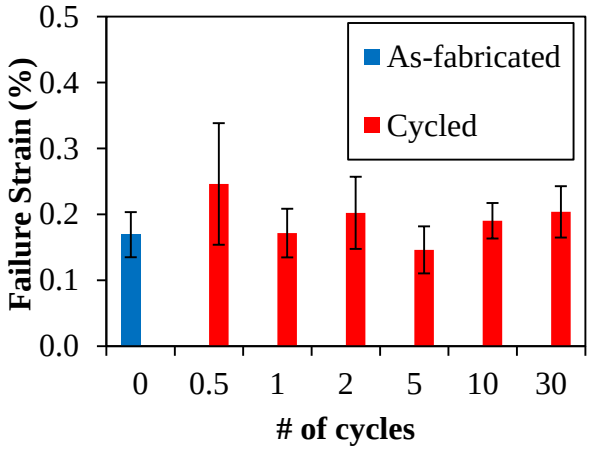

(c)

Figure 8. (a) Elastic modulus, **(b)** tensile strength, and **(c)** failure strain vs. number of electrochemical cycles for graphite anodes with 47% porosity. A full cycle includes one full lithiation and delithiation. The first two galvanostatic cycles were completed at C/30 rate and the following cycles at C/5 rate.

Sn anodes on the other hand demonstrated major degradation of their mechanical strength upon lithiation, especially for small porosity values. The ultimate strain and tensile strength vs. porosity are shown in Figures 9(a,b). The standard deviations of the average values were relatively large, reaching 50% of the average value for samples with low porosity. The large deviations were due to the considerably larger volumetric expansion of the Sn particles compared to graphite, leading to debonding and nucleation and coalescence of large voids that initiated early failure. As shown in Figure 9(b), the mechanical strength varied significantly for small porosities: the high matrix density resulted in uneven transport of the electrolyte as evidenced by variations in the delithiation capacity between cycles as different parts of the anode delithiated during each cycle, and therefore, the overall porosity increased with electrochemical cycling. Thus, small porosities, although beneficial from a mechanical integrity view point, compromise the electrochemical performance of Sn or graphite anodes.

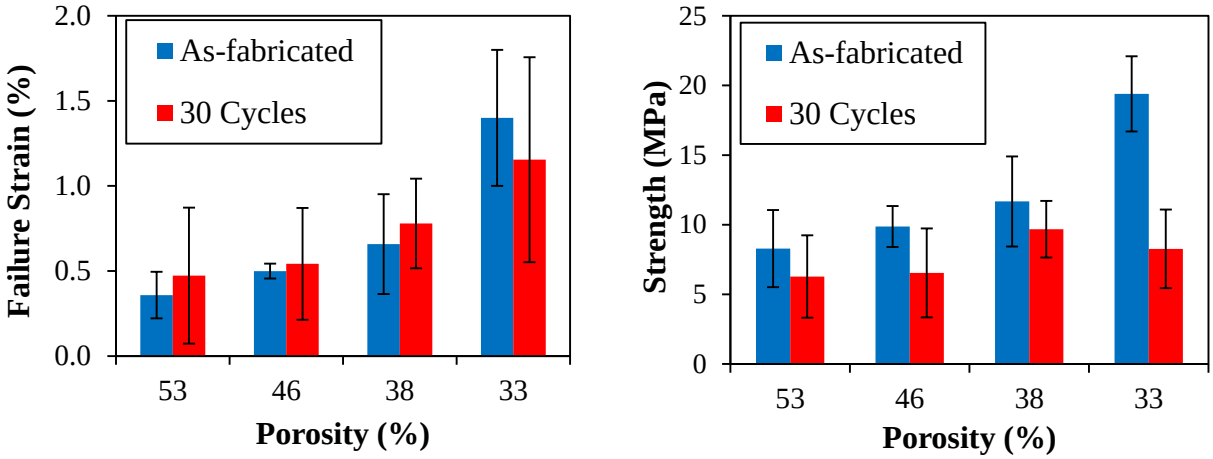

Figure 9. (a) Failure strain and **(b)** tensile strength vs. porosity of Sn anodes that are as-fabricated and electrochemically cycled for 30 full cycles.

2.3. In-situ Chemical Lithiation of Si Microsprings

Si has been shown to have very large electrochemical capacity but poor mechanical stability due to fragmentation during Li^+ intercalation. It has been shown that Si nanowires with dimensions of the order of hundreds of nanometers can avert failure while allowing for large Li^+ capacity. In this work, chemical lithiation experiments were conducted with Si microsprings of different dimensions. Specifically, four types of 10-μm thick spring films with seed spacing/number of coil turns of (a) 900 nm/4 turn, (b) 1500 nm/4 turn, (c) 900 nm/10 turn and (d) 1500 nm/10 turn, as shown respectively in Figures 10-13 were studied.

Individual springs were isolated from each film and mounted at the tip of a probe and subsequently placed in a Focused Ion Beam (FIB) chamber and brought to contact with Li metal. The surface of the latter was oxidized forming Li_2O after short exposure to air. Once the Si nanosprings were in contact with the Li_2O surface, the electron-beam was focused at the contact point causing the Li_2O to break down. Li atoms then diffused in the Si nanosprings. A necessary condition for Li_2O break-down is e-beam intensity larger than $50A/m^2$. This process of chemical lithiation [20,21] differs from electrochemical lithiation because there is no potential applied between the anode and the cathode.

Four snapshots of the lithiation process per specimen type are shown in Figures 10-13. The diffusion of Li atoms in Si nanosprings is evidenced by volume increase, starting at the contact point with the Li metal. There was no additional volume increase after the volume increase propagated to the end of each spring. The exact amount of volume increase was not possible to compute because of uncertainties in the exact geometry of each spring. During Li atom diffusion, sporadic crack formation (usually one surface crack in each spring) was observed in FIB images of the 1500 nm spaced springs of 4 and 10 turns, however no complete and catastrophic failure was observed contrary to lithiation experiments of Si films reported in literature.

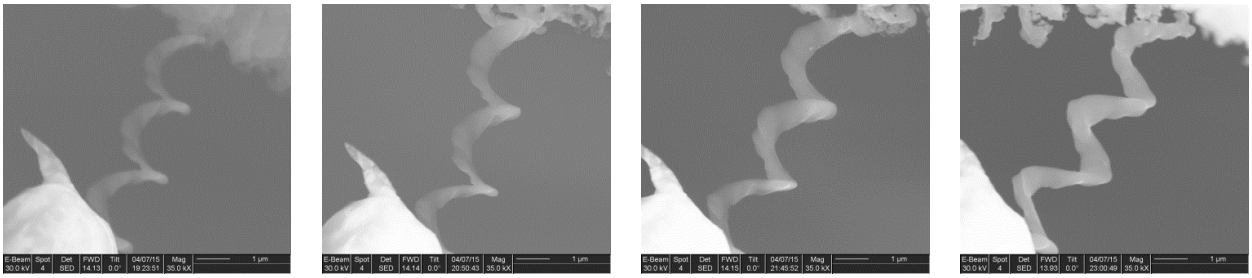

(a) **(b)** **(c)** **(d)**

Figure 10. In-situ chemical lithiation of a 900nm/4 turn Si nanospring at **(a)** 0 min, **(b)** 87 min **(c)** 144 min and (**d)** 259 min.

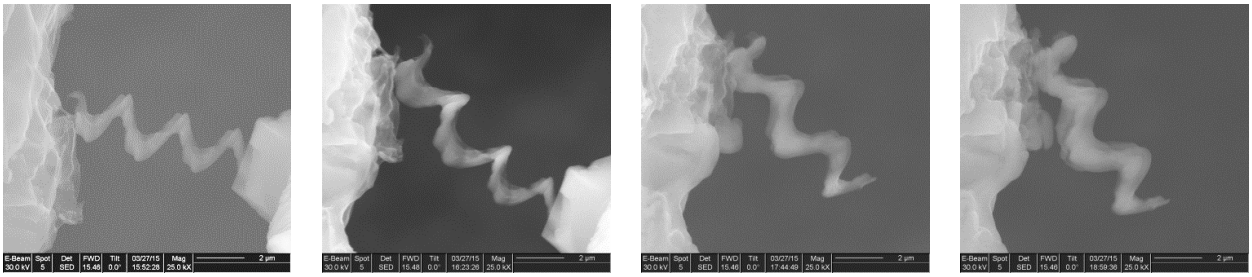

(a) **(b)** **(c)** **(d)**

Figure 11. In-situ chemical lithiation of a 1500nm/4 turn Si nanospring at **(a)** 0 min, **(b)** 31 min **(c)** 112 min and (**d)** 178 min.

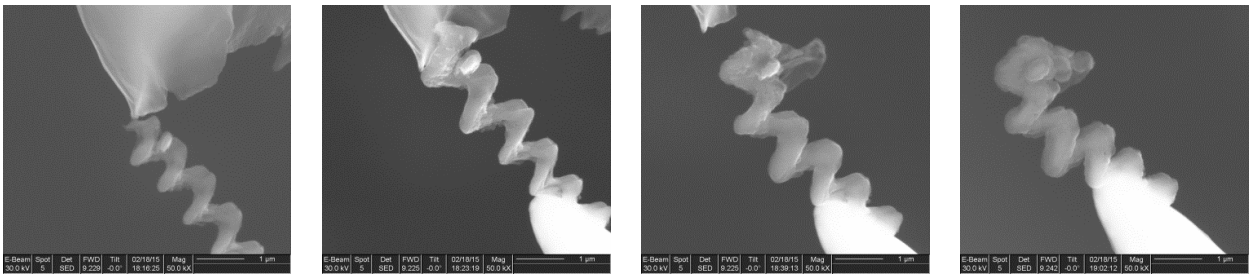

(a) **(b)** **(c)** **(d)**

Figure 12. In-situ chemical lithiation of a 900nm/10 turn Si nanospring at **(a)** 0 min, **(b)** 7 min **(c)** 23 min and (**d)** 46 min.

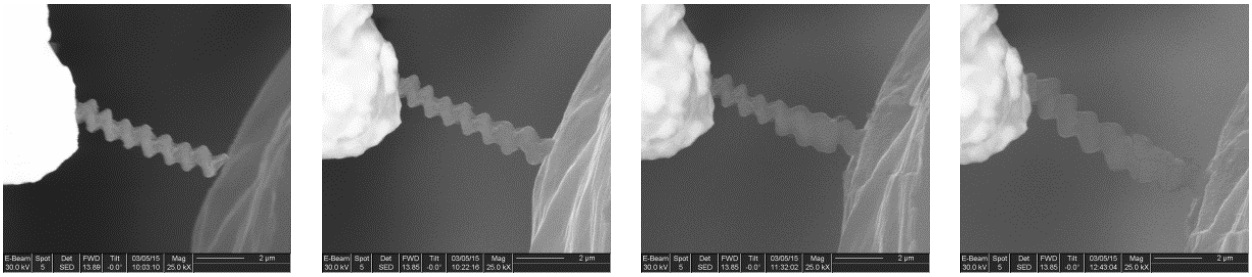

(a) **(b)** **(c)** **(d)**

Figure 13. In-situ chemical lithiation of a 1500nm/10 turn Si nanospring at **(a)** 0 min, **(b)** 19 min **(c)** 89 min and (**d)** 160 min.

References

[1] D. Antartis, I. Chasiotis, "Residual Stress and Mechanical Property Measurements in Amorphous Si Photovoltaic Thin Films", *Solar Energy* **105**, pp. 694–704, (2014).

[2] J.W. Hutchinson, Z. Suo, "Mixed-mode cracking in layered materials", *Advanced Applied Mechanics* **29**, pp. 63-191, (1992).

[3] M.D. Thouless, Z. Li, N.J. Douville, S. Takayama, "Periodic cracking of films supported on compliant substrates", *Journal of the Mechanics Physics of Solids* **59**, pp. 1927-1937, (2011).

[4] A.A. Volinsky, P. Waters, "Sub-critical telephone cord delamination propagation and adhesion measurements", *Materials Research Society Symposium Proceedings* **854E**, (2005).

[5] M.W. Moon, H.M. Jensen, J.W. Hutchinson, K.H. Oh, A.G. Evans, "The characterization of telephone cord buckling of compresses thin films on substrates", *Journal of the Mechanics Physics of Solids* **50**, pp. 2355-2377, (2002).

[6] K., Jonnagadda, I., Chasiotis, S., Yagnamurthy, J., Lambros, R., Polcawich, J., Pulskamp, M., Dubey, "Experimental Investigation of Strain Rate Dependence in Nanocrystalline Pt Films", *Experimental Mechanics* **50**, pp. 25-35, (2010).

[7] C. Gaire, D.X. Ye, F. Tang, R.C. Picu, G.C. Wang, T.M. Lu, "Mechanical Testing of Isolated Amorphous Silicon Slanted Nanorods", *Journal of Nanoscience and Nanotechnology* **5**, pp. 1893-1897, (2005).

[8] D.H. Chung, W.R. Buessem, "The Voigt-Reuss-Hill (VRH) approximation and the elastic moduli of polycrystalline ZnO, Ti2O (rutile), and α-Al2O3", *Journal of Applied Physics* **39**, pp. 2777-2782, (1968).

[9] I.B. Kobiakov, "Elastic, piezoelectric and dielectric properties of ZnO and CdS single crystals in a wide range of temperatures", *Solid State Communications* **35**, pp. 305-310. (1980).

[10] S.O. Kucheyev, J.E. Bradby, J.S. Williams, C. Jagadish, M.V. Swain, "Mechanical deformation of single-crystal ZnO", *Applied Physics Letters* **80**, pp. 956-958, (2002).

[11] C.W. Ong, D.G. Zong, M. Aravind, C.L. Choy, "Tensile strength of zinc oxide films measured by a microbridge method", *Journal of Materials Research Society* **18**, pp. 2464-2472, (2003).

[12] D. Antartis, S. Dillon, I. Chasiotis, "Effect of Porosity in Electrochemical and Mechanical Properties of Composite Li-ion Anodes", *Journal of Composite Materials*, pp. 1-14, DOI: 10.1177/0021998314568653, (2015).

[13] M.B. Pinson, M.Z. Bazant, "Theory of SEI formation in rechargeable batteries: Capacity fade, accelerated aging and lifetime prediction", *Journal of the Electrochemical Society* 160, pp. A243-A250, (2012).

[14] M. Wu, X. Xiao, N. Vukmirovic, S. Xun, P.K. Das, X. Song, P. Olalde-Velasco, D. Wang, A.Z. Weber, L.W. Wang, V.S. Battaglia, W. Yang, G. Liu, "Towards an ideal binder design for high-capacity battery anodes", *Journal of the American Chemical Society* **135**, pp. 12048-12056, (2013).

[15] S. Cho, I. Chasiotis, "Elastic properties and representative volume element of polycrystalline silicon for MEMS", *Experimental Mechanics* **47**, pp. 37-49, (2007).

[16] J. Saunier, F. Alloin, J.Y. Sanchez, L. Maniguet, "Plasticized microporous poly(vinylidene fluoride) separators for lithium-ion batteries. III. Gel properties and irreversible modifications of poly(vinylidene fluoride) membranes under swelling in liquid electrolytes", *Journal of Polymer Science* **42**, pp. 2308-2317, (2004).

[17] Z. Chen, L. Christensen, JR. Dahn, "Study of the mechanical and electrical properties of carbon/poly(vinylidene fluoride–tetrafluoroethylene– propylene) films crosslinked with triethylenetetramine: Possible application as binder for lithium-ion battery electrodes", *Journal of Applied Polymer Science* **91**, pp. 2949-2957, (2004).

[18] S. Renganathan, G. Sikha, S. Santhanagopalan, R. White, "Theoretical analysis of stresses in a lithium ion cell", *Journal of the Electrochemical Society* **157**, pp. A155-163, (2010).

[19] R. Younezi, M. Hahiln, K. Edström, "Surface characterization of the carbon cathode and the lithium anode of Li–O_2 batteries using $LiClO_4$ or LiBOB salts", *ACS Applied Materials International* **5**, pp. 133-1341, (2013).

[20] X.H. Liu, Y. Liu, A. Kushima, S. Zhang, T. Zhu, J. Li, J.Y. Huang, "In Situ TEM Experiment of Electrochemical Lithiation and Delithiation of Individual Nanostructures", *Advanced Energy Materials* **2**, pp. 722-741, (2012).

[21] J.H. Seo, C.Y. Chou, Y.H. Tsai, Y. Cho, T.Y. Seong, W.J. Lee, M.H. Cho, J.P. Ahn, G.S. Hwang, I.S. Choi, "Ultrafast chemical lithiation of single crystalline nanowires: in situ characterization and first principles modeling", *RSC Advances* 5, pp. 17438-17443, (2015).

1.

1. Report Type

Final Report

Primary Contact E-mail
Contact email if there is a problem with the report.

chasioti@illinois.edu

Primary Contact Phone Number
Contact phone number if there is a problem with the report

217-244-1474

Organization / Institution name

Aerospace Engineering, University of Illinois at Urbana-Champaign

Grant/Contract Title
The full title of the funded effort.

Influence of Mechanical Loading on the Integrity and Performance of Storage Materials at the Micron and Submicron Scales

Grant/Contract Number
AFOSR assigned control number. It must begin with "FA9550" or "F49620" or "FA2386".

FA9550-12-1-0209

Principal Investigator Name
The full name of the principal investigator on the grant or contract.

Ioannis Chasiotis

Program Manager
The AFOSR Program Manager currently assigned to the award

Dr. B.L. Lee

Reporting Period Start Date

06/15/2012

Reporting Period End Date

12/14/2015

Abstract

The mechanical reliability and efficiency of thin film photovoltaics attached to structural members depends on the initial residual stresses in the films. In this research, accurate predictions of the mechanical and functional failure of photovoltaic films co-cured on carbon fiber composite laminates were made possible by quantifying the mean and gradient residual stresses and the failure properties of individual layers in thin film amorphous Si photovoltaics. The experimental results were employed to predict the onset of fragmentation in the transparent conductive oxide ZnO layer and the amorphous Si and the initiation of functional degradation of photovoltaic films co-cured on 0˚ carbon fiber composite laminates. In parallel, this research program investigated the electrochemical and mechanical performance of graphite and Sn composite anodes subjected to electrochemical cycling. Most composite anodes reported in literature are very porous because they are manufactured from slurry, and as a result, they have no mechanical integrity. The composite graphite and Sn anodes fabricated in this research were prepared by hot pressing which allowed for control of their porosity between 35% and 75%. Porosities larger than 45% preserved the electrochemical capacity of the anodes, as opposed to those with porosities smaller than 40% that had reduced electrochemical capacity. Graphite anodes with ~45% porosity demonstrated the highest retention of tensile strength and elastic modulus after 30 electrochemical cycles, representing an optimum condition.

Finally, the fracture of Si as high capacity Li+ host material was investigated using Si microsprings. Experiments conducted under purely chemical lithiation, showed good lithiation and small propensity for crack formation, thus making films of such springs a viable material for high capacity thin film anodes.

Distribution Statement

This is block 12 on the SF298 form.

Distribution A - Approved for Public Release

Explanation for Distribution Statement

If this is not approved for public release, please provide a short explanation. E.g., contains proprietary information.

SF298 Form

Please attach your SF298 form. A blank SF298 can be found here. Please do not password protect or secure the PDF
The maximum file size for an SF298 is 50MB.

Form 298_04-01-2016.pdf

Upload the Report Document. File must be a PDF. Please do not password protect or secure the PDF . The maximum file size for the Report Document is 50MB.

Final_Report_04-01-2016.pdf

Upload a Report Document, if any. The maximum file size for the Report Document is 50MB.

Archival Publications (published) during reporting period:

D. Antartis, S. Dillon, I. Chasiotis, "Effect of Porosity in Electrochemical and Mechanical Properties of Composite Li-ion Anodes", Journal of Composite Materials, pp. 1-14, DOI: 10.1177/0021998314568653, (2015).

D. Antartis and I. Chasiotis, "Residual Stress and Mechanical Property Measurements in Amorphous Si Photovoltaic Thin Films", Solar Energy 105, pp. 694–704, (2014).

Changes in research objectives (if any):

NONE

Change in AFOSR Program Manager, if any:

N/A

Extensions granted or milestones slipped, if any:

A no cost extension of 6 months was granted and completed.

AFOSR LRIR Number

LRIR Title

Reporting Period

Laboratory Task Manager

Program Officer

Research Objectives

Technical Summary

Funding Summary by Cost Category (by FY, $K)

	Starting FY	FY+1	FY+2
Salary			
Equipment/Facilities			
Supplies			
Total			

Report Document

Report Document - Text Analysis

Report Document - Text Analysis

Appendix Documents

2. Thank You

E-mail user

Apr 01, 2016 15:08:09 Success: Email Sent to: chasioti@illinois.edu